THE RESULTS OF ANALYSES OF LMFBR FUEL ROD CLADDING TO PREDICT FAILURE UNDER PROTOTYPIC LOADING CONDITIONS

R.G. SIM, S. VAIDYANATHAN

Breeder Reactor Department, Nuclear Energy Division,
General Electric Company, Sunnyvale, California 94086, U.S.A.

SUMMARY

The failure mechanisms for mixed oxide fuel rods in a fast flux/flowing sodium environment are ill-defined. There are many loading mechanisms which might contribute to the failure of a rod. Out of these loading mechanisms the fuel to clad interaction problem has received the most attention with the others being almost totally neglected. The results reported here are part of a program of analyses directed towards evaluating the relative importance of these other clad loading mechanisms for typical reactor operating histories. The loading mechanisms considered include the internal fission gas pressure, the wastage of the clad wall thickness, the contact loads due to spacer restraint and the thermal and differential swelling stresses which result from considering prototypic temperature distributions.

Analyses have been conducted using a variety of tools. The fission gas, the wall thinning and the temperature effects were analyzed using a two-dimensional generalized plane strain code called GOGO. The GOGO code solves the problem on a closed form basis except for some terms which are evaluated by numerical integration. The contact load problem was analyzed using the CREEP-PLAST (two-dimensional plane strain model) and the MARC-CDC (three-dimensional model) finite element codes.

Using the GOGO code it has been found that the effect of the thermal stresses is not very important for steady power operation. However, the differential swelling which occurs can, in certain cases, cause an order of magnitude more creep rupture damage than would occur due to the fission gas pressure alone. Also under conditions of typical reactor power and flow cycling it has been found that variations in the thermal stresses which result under these conditions can cause enhancement of the end of life creep strains as well as causing an equal number of cycles of tensile and compressive creep at certain locations in the clad. The latter phenomenon is a type of low cycle fatigue and is the more significant of the two phenomena. The extent of the fatigue damage is dependent on the magnitude of the thermal stresses and the number, magnitude, and duration of the power cycles. The prediction of failure under these conditions of creep-fatigue interaction is difficult due to shortages of totally applicable data. However damage estimates indicate that this type of damage mechanism might be a real limitation to reactor operation. These results emphasize the importance of considering in analyses the effect of the radial and the circumferential variation of the temperature in the clad.

The conclusions of the work on spacer contact loads are summarized.

1.0 INTRODUCTION

A list of loading mechanisms for LMFBR fuel rod cladding are given in Table 1. Using typical LMFBR design parameters and simple analysis procedures these loading mechanisms were classified according to their potential to cause clad failure. In general the fuel to clad interaction loads have received considerable attention. This paper reports the results of an evaluation of the loading mechanisms in Table 1 which are not due to the fuel and which fall under the 'important' or 'not known' classification. The purpose of the evaluation was to determine first the loading mechanisms which are important in design and second the analytical tools required to correctly model the identified loading mechanisms.

The interaction between the fission gas pressure, the radial, circumferential and the hot spot temperature gradients and the clad thickness wastage were analysed using a code called GOGO. The effect of spacer contact loads was analyzed using the MARC-CDC and the CREEP PLAST finite element codes. All the analyses were conducted for 20% cold worked type 316-stainless steel rods operating in a typical LMFBR core which has a 720°F inlet and 1000°F mixed mean outlet temperature.

2.0 DESCRIPTION OF COMPUTER CODES USED

2.1 GOGO

GOGO is a special purpose code which solves two dimensional generalized plane strain fuel rod cladding problems. The solution procedure is the same as that described by Penny and Sim [1] but extended to two dimensions and for generalized plan strain conditions. The code treats fission gas pressure, radial displacements at the inside boundary of the clad, prototypic clad temperature distributions and the wastage of the clad wall thickness. Variable loading effects due to burnup changes or reactor power and flow variations can easily be modeled using the code. Elastic material behavior, thermal expansion effects, radiation creep, thermal creep and metal swelling are all analysed by the code. In addition,the damage in the clad is evaluated on four different bases as given below:

1. life fraction based on the effective stress [denoted by $lf(\bar{\sigma})$]
2. life fraction based on the maximum principal tensile stress [denoted by $lf(\sigma_M)$]
3. strain fraction based on the positive increments of effective thermal creep strain [denoted $sf(\Delta\epsilon)$]
4. strain fraction based on the absolute increments of effective thermal creep strain [denoted $sf(|\Delta\epsilon|)$]

It is important to note that only thermal creep is considered damaging; the radiation creep is considered to be non-damaging being limited to allowable strains significantly greater than the limits for thermal creep. Failure is nominally considered to occur when the damage fractions equal unity. The nomenclature established above to denote the damage values is used throughout the paper.

2.2 MARC-CDC and CREEP-PLAST

The MARC-CDC Code by the MARC Analysis Corporation [2] and the CREEP-PLAST code by Rashid [3] are both finite element codes. Both codes treat elasticity, plasticity, thermal expansion, radiation creep, thermal creep and swelling. The doubly curved shell element of the MARC-CDC code was used to model the cladding. The CREEP-PLAST code was operated in a plane strain mode using constant strain triangular elements.

3.0 ANALYSIS

3.1 Clad Behavior due to Fission Gas, Clad Wastage and Prototypic Temperature Distributions

Analyses were carried out to investigate the effect on the clad of the interaction of the fission gas pressure, the clad thinning and the radial, circumferential and hot spot temperature gradients for steady and varying power operation. Table 2 gives the typical operating conditions for a hot, a peak power, an average power and a minimum power rod located in the edge row of a 217 rod bundle. The temperature distribution in the clad was calculated using the equation in Table 2. The fuel rods remain in the core for two refueling cycles. To simplify the problem the clad and core ΔT's were assumed to remain constant during each cycle of operation with those in the second cycle being reduced by the amount indicated in Table 2 to account for burnup. The fission gas pressure and the clad thickness wastage were assumed to vary linearly with life with an adjustment being made during the second cycle to reflect the lower temperature.

3.1.1 Steady Power Operation

Both one and two dimensional calculations were carried out. The two dimensional model was a 180° clad section with 10 radial sections and 20 segments around the circumference. All the results are based on 20% cold worked type 316 stainless steel design correlations which include the effect of the radiation and flowing sodium environment where appropriate. The results are presented in Table 3. For the minimum and average power rods the table shows that failure is extremely unlikely due to the loading conditions considered. The peak power and the hot rods which operate nearer to the design limiting conditions were analysed in more detail. For these two rods four calculations were carried out at each axial location. All four calculations had the same maximum midwall temperature, fission gas and clad wastage history; the only difference being the extent of the variation of the temperature distribution within the clad. The base case assumed that the rod was a thin wall tube at a temperature equal to the maximum midwall temperature in the cladding. The other three cases analysed the clad as a thick-walled tube. The damage values in Table 3 for the thin wall isothermal case are a measure of the damage due to internal pressure alone. The difference in the damage values between this base case and the other cases are then due to the presence of the temperature gradients. The temperature gradients cause increased damage in two ways:

1. They give rise to thermal stresses which can contribute to life fraction damage and if relaxed strain fraction damage.
2. The differential swelling which occurs due to the temperature differences causes increased stresses and strains which contribute to the life fraction and the strain fraction damage values.

The principal causes of the peak damage values have been identified in Table 3. When the damage is principally caused by differential swelling, the area of high damage is limited. This result is illustrated by Figure 1 which shows the area of the clad section at the core midplane in the hot rod which has an end-of-life damage value greater than 1. This result is for the case where all the temperature gradients are included in the analysis. It is evident that although the peak damage in this case is extremely high (2270) the region where failure might be reasonably expected [$1f(\sigma_M)>1$] is extremely localized and would not be expected to cause a through-the-wall crack in the clad. This result is in contrast to the distribution of damage in the same rod at the top of the core. In this case although the peak damage is much lower (2.5) since the principal cause of damage is internal pressure, the damage is more evenly distributed and would cause a through-the-wall crack. The same conclusions are evident from Figures 3 and 4 which for the same cases just discussed illustrate the distribution of the effective thermal plus radiation creep strain. From Figure 3 for the hot rod at the core midplane, the strains are quite evidently due to secondary stresses. Whereas in Figure 4 it is evident that the strains have been caused by a primary stress system.

These results indicate that in general a through-the-wall crack in the clad may be reasonably, if somewhat nonconservatively, predicted by considering only the internal pressure and assuming the clad to be an isothermal thin wall tube with a temperature equal to the maximum midwall temperature in the clad. However, it is evident that differential swelling due to temperature differences in the clad may cause localized cracking in the clad usually on the outside surface. The appearance of swelling enhanced radiation creep would not be expected to entirely relieve this situation since the peak radiation creep strains ($\sim$3%) would be such that the superplasticity of stainless steel would be seriously in question. This cracking allied to the fission product cracks on the inside of the clad may seriously degrade the clads ability to withstand other loading conditions.

3.1.2 Cyclic Power and Flow Operation

Equal power and flow variations within the core of a LMFBR cause proportional changes in the radial, circumferential and hot spot temperature gradients within the clad while the average clad temperature remains unchanged. Analysis was carried out to determine the effect of such cyclic power and flow changes on the hot and peak power cladding. Two cases were analyzed. In both cases the power and flow were reduced from 100% to 35% for 50 hours. This cycle was repeated every 500 hours in one case and every 1000 hours in the other. In each case the rod continued operating until it had reached a

fluence equal to that it would have had under the 100% steady power operation discussed previously.

The analyses included the effect of fission gas, clad thinning and the radial, circumferential and hot spot temperature gradients. Table 4 tabulates the results for the two rods for both the cyclic and the steady power operation. At the core midplane the life fraction values decrease due to the longer time available for creep to relax the differential swelling stresses. At the top of the core the life fraction values increase since the continual fluctuation of thermal stress means that the clad experiences a higher average stress during its life. The most revealing changes are in the strain fraction values. At the core midplane there is very little change. This is expected since the thermal stress effects due to cycling are small relative to the differential swelling stresses and thermal creep is relatively inactive at these lower temperatures. However, at the top of the core increased damage fractions are observed with the change being greatest in the case of the hot rod. The change in the $sf(\Delta\varepsilon)$ value in the hot rod is simply due to the longer times spent at pressure. This effect is not significant for the peak rod since internal pressure is not a principal cause of damage. The change in the $sf(|\Delta\varepsilon|)$ value for both the peak and hot rod reflects the longer thermal creep strain path due to cyclic loading. Such an increase occurs due to the repeated relaxation of the thermal stresses which reverse at each change in power.

The difference between the $sf(\Delta\varepsilon)$ value and the $sf(|\Delta\varepsilon|)$ is an indication of the fatigue damage suffered by the clad. Figure 5 shows this effect plotted in terms of the effective thermal creep strain versus the number of cyclic power and flow variations. From Figure 5 it is seen that for each cycle from 100% to 35% power and flow for 50 hours the peak thermal creep strain path is increased by approximately 0.05%. Prediction of failure due to such creep-fatigue interaction in irradiated cladding is difficult. More data and improved damage and failure criteria are required. However, these results do indicate that the damage in the higher temperature (>1200°F) cladding will increase in proportion to the number and the magnitude of cyclic power and flow variations. The time spent at each power level is also a variable which effects the total fatigue damage.

3.2 Clad to Spacer Contact Loads

It has been predicted based on bundle compression test data that the differential expansion between the fuel rod bundle and its surrounding channel in a typical LMFBR core may give clad contact loads as high as 14 lbs for a peak bundle to channel interaction of 66 mils. An analysis was carried out using the MARC-CDC code to evaluate the importance to clad failure of such high contact loads. The problem case modeled is shown in Figure 6. It corresponds to a 6 inch section of a corner rod in a 217 rod bundle. 816 isoparametric curved triangular shell elements were used to three dimensionally model the rod. Three loads act on the rod. The largest load is due to the interaction between the corner rod and the other 16 rods across the corners of the bundle. The smaller loads occur where the corner rod contacts the two rows of rods parallel to channel sides. The loads were applied in three equal increments as shown in Figure 7

over a total loading period of 6300 hours . The pressure within the rod was assumed to remain constant at 300 psi. The temperature of the design case studied was low enough (990°F) that thermal creep effects can be neglected. The elastic deflections of the clad agreed with these calculated from Roark [4]. Under loading the clad deformed due to radiation creep. The local deflection history is shown in Figure 7. The maximum end-of-life total (elastic and creep) local cladding indentation under the spacer was of the order of 1.2 mils and the maximum radiation creep strains are of the order of 0.5%. Although such a local indentation is small, the sum of the indentations across a 217 rod bundle is significant and would be expected to reduce the predicted peak load based on room temperature bundle compression tests by about 25%.

The two dimensional CREEP-PLAST code was used to model the local load effect. A plane section model with a line load parallel to the axis of the rod was analyzed. For the same elastic deflection the CREEP-PLAST model confirmed the results of the MARC-CDC code.

It is expected that the limiting condition for contact loads at temperatures less than 1050°F will be local yielding due to high local stresses. The presence of typical fission product intergranular cracks at the inside surface of the cladding while a contact load is acting is not expected to initiate unstable crack propagation even for fluences as high as 2×10^{23} nvt (>0.1 Mev) in stainless steel.

4.0 CONCLUSIONS

Under steady loading the main effect of the temperature gradients in the clad is to cause differential swelling. At high fluences such differential swelling may result in localized cracking at the outer surface of the clad. Under cyclic power and flow conditions the thermal stresses due to the changing temperature gradients may cause significant low cycle fatigue damage in the higher temperature clad where thermal creep is active.

The radiation creep indentations in cladding due to contact loads may be expected to reduce by about 25% the peak loads calculated on an elastic basis only.

REFERENCES

[1] Penny R.K. and Sim R.G. "Time dependent creep of plates and pressure containers" Proc. 1st Int. Conf. Pressure Vessel Technology Vol. II 845 (1969)

[2] MARC Analysis Corporation "Users Information Manual MARC-CDC Volume I-III" issued by Control Data Corporation

[3] Rashid Y.R. "Part II Users Manual for CREEP-PLAST Computer Program" GEAP 13262 March 1972.

[4] Roark R.J. "Formulas for Stress and Strain" McGraw Hill

Table 1 - Loading Mechanisms for LMFBR Fuel Rod Cladding Listed According to their Potential to Cause Clad Failure

	Important	Not Known	Not Important
1. Pressure at inner boundary due to fuel/clad interaction	F		
2. Pressure at inner boundary due to fission gas pressure	NF		
3. Radial temperature gradient through the wall	NF		
4. Circumferential temperature gradient across the rod	NF		
5. Hot Spot temperature gradient	NF		
6. Axial temperature gradients			NF
7. Second order circumferential temperature variations due to local variations in coolant flow			NF
8. Clad thickness wastage (sodium corrosion, fretting and wear, fuel/clad intergranular attack)	NF		
9. Contact loads due to wire wrap or grid spacer systems		NF	
10. Asymmetric fuel loads (pellet discontinuities and cracking)		F	
11. Axial loading of the clad by fuel		F	
12. End plug effects			NF
13. Fatigue damage due to rod vibration			NF

F - load due to fuel
NF - load not due to fuel

Table 2 Typical LMFBR Fuel Rod Cladding Operating Conditions where Coolant inlet temperature is 720°F and mixed mean outlet temperature equals 1000°F. (0.23 inch diameter rods in edge row of 217 rod bundle)

	Hot Rod		Peak Power Rod		Average Power		Minimum Power	
	Top of Core	Core ℄	Top of Core	Core ℄	Top of Core	Core ℄	Top of Core	Core ℄
Maximum Midwall Temperature BOL[1] (°F)	1372	1173	1231	1085	1014	982	980	917
Average Temperature BOL, T_{avg} (°F)	1279	1044	1115	976	992	904	919	860
ΔT through wall, ΔT_{wall} (°F)	65	108	56	100	41	74	35	62
ΔT across rod, ΔT_{rod} (°F)	114	132	165	100	114	70	81	50
ΔT Hot spot, ΔT_{hot} (°F)	42	74	39	69	29	51	24	42
Wall thickness BOL (mils)	15	15	15	15	15	15	15	15
Wall thickness EOL[2] (mils)	12.25	13.01	13.63	13.58	14.55	14.41	14.76	14.71
Fission gas pressure BOL(psi)	97	97	88	88	81	81	77	77
Fission gas pressure EOL(psi)	931	931	798	798	648	648	445	445
Ratio of power in second cycle to power in 1st cycle	0.815	0.815	0.825	0.825	0.85	0.85	0.827	0.827
On power life (hrs)	13154	13154	13154	13154	13154	13154	13154	13154

1 BOL = Beginning of Life

2 EOL = End of Life

$$T = T_{avg} + \Delta T_{wall}\,\frac{r_i + r_o - 2r}{2\,(r_o - r_i)} + \Delta T_{rod}\,\frac{\sin(\theta)}{2} + \Delta T_{hot}\left[1 - \frac{0.3(r_o - r)}{r_o - r_i}\right]\exp(-6.5\chi)$$

where χ = absolute angular distance from hot spot in radians

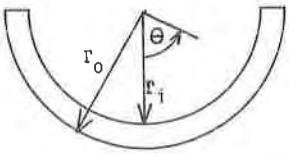

Table 3 Peak End-of-Life Damage Values for Steady Power Rod Operation

	End-of-Life Peak Damage Values					
	$sf(\Delta\varepsilon)$	$sf(\lvert\Delta\varepsilon\rvert)$	Principal Cause	$lf(\bar{\sigma})$	$lf(\sigma_M)$	Principal Cause
Hot Rod - Tof of Core						
$\Delta T_{wall}+\Delta T_{rod}+\Delta T_{hot}$	1.22	1.94	1, 2	3.1	2.5	1, 3
$\Delta T_{wall}+\Delta T_{rod}$	1.2	1.9		3.6	3	
ΔT_{wall}	1.24	1.58		3.4	3.2	
Isothermal thin wall	1.07	1.07	1	0.36	0.53	1
Hot Rod - Core Midplane						
$\Delta T_{wall}+\Delta T_{rod}+\Delta T_{hot}$	1.19	1.49	2, 3	186	2270	3
$\Delta T_{wall}+\Delta T_{rod}$	1.81	2.05		2.2	3	
ΔT_{wall}	1.32	1.42		1.47	1.6	
Isothermal thin wall	6×10^{-5}	6×10^{-5}	1	5×10^{-5}	7×10^{-5}	1
Peak Rod - Top of Core						
$\Delta T_{wall}+\Delta T_{rod}+\Delta T_{hot}$	0.189	0.212	2	0.029	0.024	3
$\Delta T_{wall}+\Delta T_{rod}$	0.182	0.218		0.04	0.034	
ΔT_{wall}	0.029	0.042		0.015	0.016	
Isothermal thin wall	4×10^{-4}	4×10^{-4}	1	4×10^{-4}	6×10^{-4}	1
Peak Rod - Core Midplane						
$\Delta T_{wall}+\Delta T_{rod}+\Delta T_{hot}$	0.03	0.038	3	31	2940	3
$\Delta T_{wall}+\Delta T_{rod}$	0.034	0.048		5.6	49	
ΔT_{wall}	0.042	0.044		0.025	0.033	
Isothermal thin wall	2×10^{-7}	2×10^{-7}	1	4×10^{-8}	6×10^{-8}	1
Average Rod						
ΔT of core $\Delta T_{wall}+\Delta T_{rod}+\Delta T_{hot}$	0.0026	0.0026	2	2×10^{-4}	2×10^{-8}	2
Core midplane $\Delta T_{wall}+\Delta T_{rod}+\Delta T_{hot}$	0.00023	0.00023	3	10^{-4}	2×10^{-8}	3
Minimum Rod						
Top of Core $\Delta T_{wall}+\Delta T_{rod}+\Delta T_{hot}$	10^{-6}	10^{-6}	2	10^{-7}	10^{-11}	2
Core midplane $\Delta T_{wall}+\Delta T_{rod}+\Delta T_{hot}$	10^{-8}	10^{-8}	2	10^{-9}	10^{-13}	2

1 - internal pressure

2 - initial thermal stresses

3 - differential swelling

Table 4 Peak-End-of-Life Damage Values in the Clad under Cyclic Power and Flow Conditions

Damage Fract. Values Used	Hot Rod						Peak Power Rod					
	Top of Core			Core Midplane			Top of Core			Core Midplane		
	100% power	13 cycl.	28 cycl.	100% power	13 cycl.	28 cycl.	100% power	13 cycl.	28 cycl.	100% power	13 cycl.	28 cycl.
$1f(\bar{\sigma})$	3.1	7.9	9.4	186	107	73	.029	0.11	.161	31	32	24
$1f(\sigma_M)$	2.5	5.2	4.5	2270	1250	843	.024	0.25	.389	2940	3040	2160
$sf(\Delta\epsilon)$	1.22	3.4	4	1.19	1.26	1.16	.189	.207	.214	.03	.04	.044
$sf(\lvert\Delta\epsilon\rvert)$	1.94	5	7.3	1.49	1.45	1.3	.212	.274	0.3	.038	.05	.05

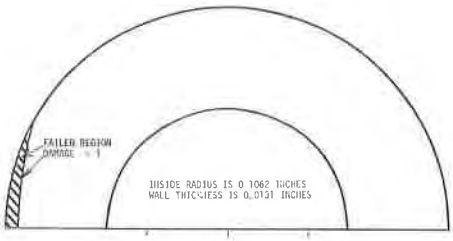

FIGURE 1 DAMAGE [$1f(\sigma_M)$] DISTRIBUTION IN THE CLAD AT THE CORE MIDPLANE OF THE HOT ROD AT THE END-OF-LIFE

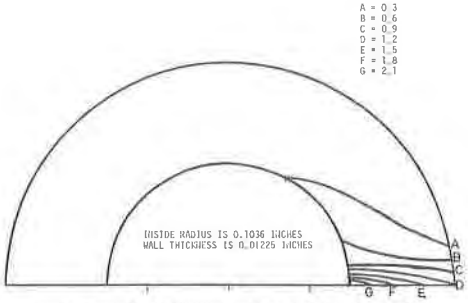

FIGURE 2 DAMAGE [$1f(\sigma_M)$] DISTRIBUTION IN THE CLAD AT THE TOP OF THE CORE IN THE HOT ROD AT THE END-OF-LIFE

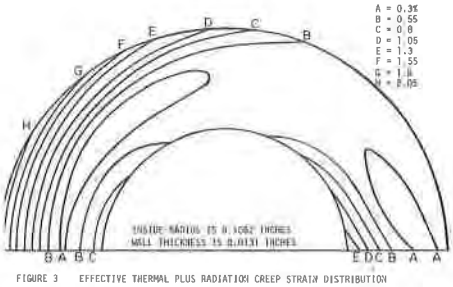

FIGURE 3 EFFECTIVE THERMAL PLUS RADIATION CREEP STRAIN DISTRIBUTION IN THE CLAD AT THE CORE MIDPLANE OF THE HOT ROD AT THE END-OF-LIFE

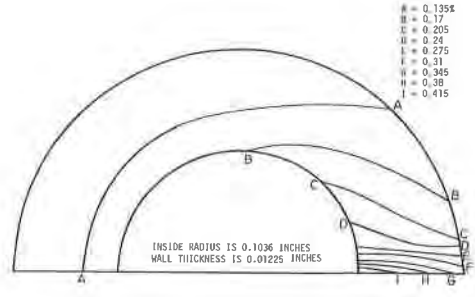

FIGURE 4 EFFECTIVE THERMAL PLUS RADIATION CREEP STRAIN DISTRIBUTION IN THE CLAD IN THE HOT ROD AT THE END-OF-LIFE

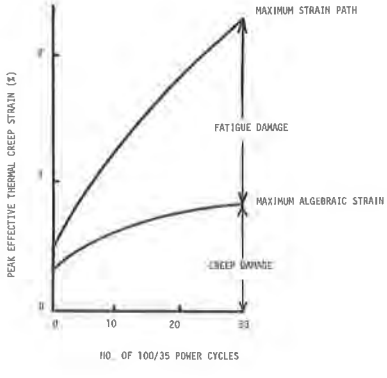

FIGURE 5 PEAK EFFECTIVE THERMAL CREEP STRAIN AND STRAIN PATH IN THE HOT ROD CLADDING AT THE TOP OF THE CORE

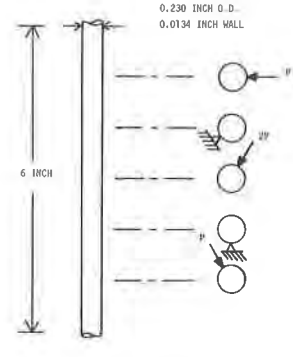

FIGURE 6 CLAD CONTACT LOAD PROBLEM: SECTION OF CORNER ROD MODELLED THREE-DIMENSIONALLY USING 816 ELEMENTS

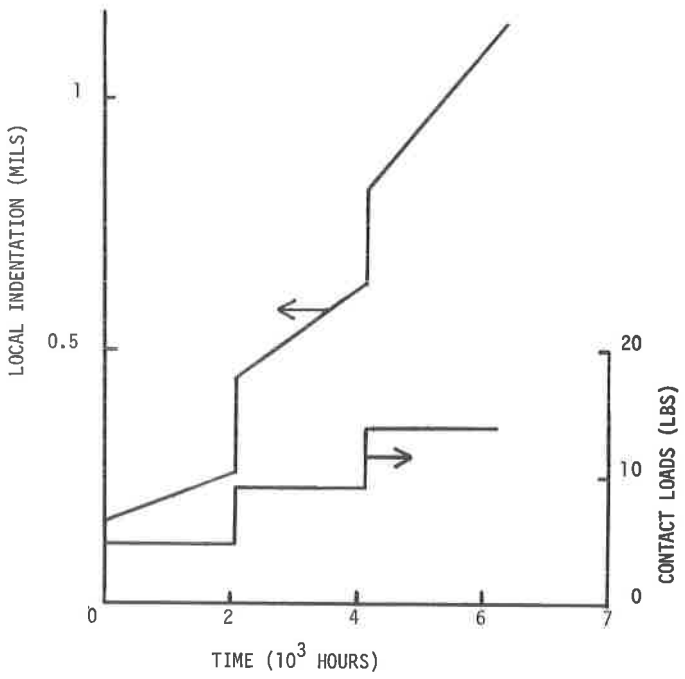

FIGURE 7 LOCAL INDENTATION IN CLAD WITH TIME DUE TO THE CONTACT LOAD